

Synthetic differential emission measure curves of prominence fine structures

S. Gunár¹, P. Heinzel¹, and U. Anzer²

¹ Astronomical Institute, Academy of Sciences of the Czech Republic, 25165 Ondřejov, Czech Republic
e-mail: gunar@asu.cas.cz

² Max-Planck-Institut für Astrophysik, Karl-Schwarzschild-Strasse 1, 85740 Garching, Germany

Received 20 October 2010 / Accepted 18 January 2011

ABSTRACT

Aims. We use 2D single and multi-thread prominence fine-structure models to obtain the synthetic DEM curves. These are then compared with the DEM curves derived from observations.

Methods. We use the temperature and electron density structure resulting from the 2D models and numerically compute the average synthetic DEM curves for different orientations of the threads with respect to the line of sight.

Results. We show that the synthetic DEM curves obtained by 2D modelling are similar to the DEM curves derived from observations of quiescent prominences.

Conclusions. The DEM curves derived from observations, which are most reliable above temperatures of 20 000 K, can be extended towards cool prominence-core temperatures by supplementing them with synthetic DEM values obtained by modelling hydrogen Lyman spectra originating mainly at temperatures below 20 000 K. On the other hand, the observed DEM can constrain the temperature structure of the prominence fine structures above the formation temperatures of the Lyman spectrum.

Key words. Sun: filaments, prominences – techniques: spectroscopic – methods: numerical

1. Introduction

Solar prominences are dense and cool structures, with typical temperatures of 6000 to 8000 K, suspended in predominantly horizontal magnetic fields within a very hot coronal environment with temperatures above 1 million K (see e.g. Tandberg-Hanssen 1995). The region surrounding the cool core of a prominence where the temperature rises from central low values towards the coronal ones is usually called the Prominence-Corona Transition Region (PCTR). Spectral lines emitted at PCTR temperatures lie in the UV and EUV range and many of these lines were observed onboard past (Orrall & Schmahl 1976; Engvold 1988) and recent space-born missions (Patsourakos & Vial 2002). The spectroscopic analyses of these lines provide useful insight into the understanding of the thermodynamic parameters of the prominence plasma, including the temperature structure of the PCTR and as such they are frequently studied (see e.g. review by Labrosse et al. 2010).

One of the widely studied quantities is the differential emission measure (DEM), which gives information on the distribution of the plasma as a function of the temperature along a given line of sight (LOS) but does not allow us to determine the spatial characteristics of the plasma LOS distribution. Assuming a region with a monotonic variation of temperature, the DEM curve is usually defined along a given LOS (h) as (see e.g. Mariska 1992; Phillips et al. 2008)

$$\text{DEM}(T) = n_e^2 \frac{dh}{dT}, \quad (1)$$

where n_e is the electron density at the LOS position h with a given temperature T . The DEM is related to the integrated

intensity I of an optically thin line through the equation

$$I = \int_0^\infty A(X) G(T) \text{DEM}(T) dT, \quad (2)$$

where $A(X)$ is the element abundance with respect to hydrogen and $G(T)$ is the contribution function for a given spectral line. This allows the derivation of the DEM from sets of observed optically thin UV and EUV spectral lines (see e.g. Wiik et al. 1993; Cirigliano et al. 2004; Parenti & Vial 2007) using inversion techniques such as those available in the CHIANTI software (see e.g. Parenti & Vial 2007; Phillips et al. 2008). The DEM can be also obtained by theoretical modelling of the prominence PCTR (see e.g. work by Chiuderi Drago et al. 1992; Anzer & Heinzel 1999, 2000; and Anzer & Heinzel 2008). These authors focused on the study of synthetic DEM values obtained by using vertical 1D slab models in MHS equilibrium (Anzer & Heinzel 2008) or an ensemble of horizontal magnetic flux tubes (Chiuderi Drago et al. 1992). In this work, we use the more realistic 2D prominence fine-structure models developed by Heinzel & Anzer (2001), which represent individual prominence fine-structure 2D threads in magneto-hydrostatic (MHS) equilibrium, including prescribed PCTR temperature structure. The 2D non-LTE radiative transfer problem is solved to obtain the synthetic hydrogen spectra of these threads. In previous papers, we demonstrated the ability of these 2D models to reproduce the observed hydrogen Lyman spectra. Gunár et al. (2007) compared the observed and synthetic Lyman spectra on a profile-to-profile basis and concluded that a multi-thread modelling is needed to obtain good agreement of the synthetic Lyman line profiles with the observed spectra. Gunár et al. (2008) demonstrated the ability of these 2D multi-thread models to reproduce also the asymmetries of the Lyman line profiles.

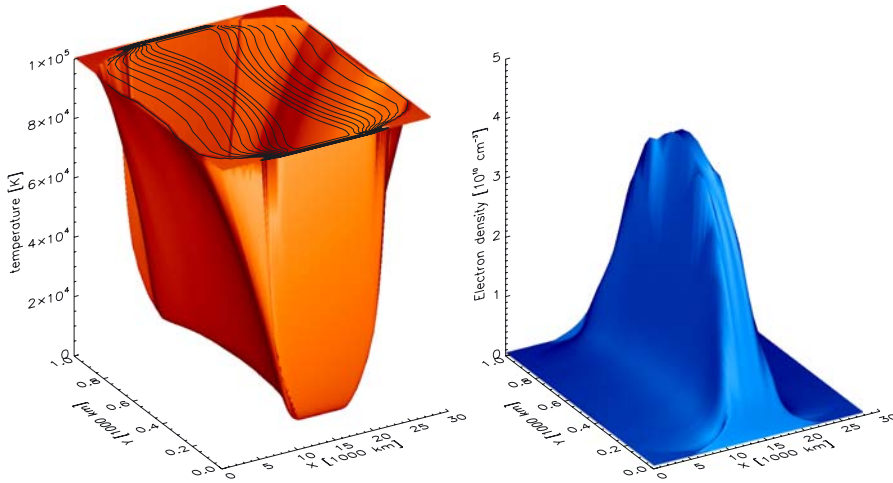


Fig. 1. MODEL1 temperature (*left side*) and electron density (*right side*) variation in the x - y plane. Note that these plots are not drawn at the proper geometrical scale.

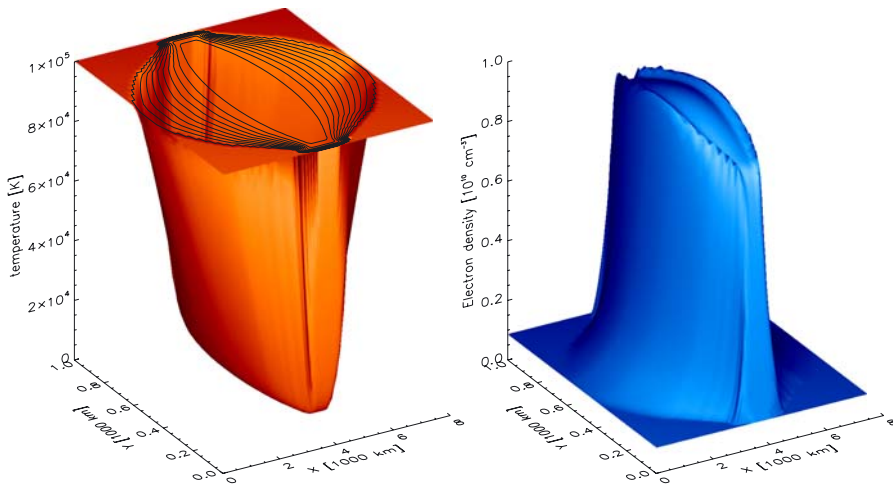


Fig. 2. MODEL2 temperature (*left side*) and electron density (*right side*) variation in the x - y plane.

Gunár et al. (2010) compared the observed and synthetic Lyman spectra on a statistical basis and showed that the large set of Lyman line observations can be reproduced by multi-thread models with a given set of plasma parameters.

In the present study, we use the temperature and electron density structures (see Figs. 1 and 2) resulting from our models to derive the synthetic DEM curves corresponding to single-thread and the multi-thread 2D prominence fine structure models.

The paper is organized in the following way: in Sect. 2 we give a brief description of our prominence fine-structure models and their parameters; in Sect. 3 we present the numerical method for deriving the synthetic DEM and the resulting DEM curves derived from selected models; and in Sect. 4 we give the discussion and present our conclusions.

2. Prominence fine-structure models

We employ the 2D models of the prominence fine-structure threads in both single-thread and multi-thread configurations. These 2D models were developed by Heinzel & Anzer (2001) and represent the prominence fine structures in a form of 2D vertically infinite threads embedded in a horizontal magnetic field. The variation in all quantities takes place only in the horizontal plane. The 2D threads are in a magnetohydrostatic (MHS) equilibrium of Kippenhahn and Schlüter type (Kippenhahn & Schlüter 1957) that was generalized to 2D by Heinzel & Anzer (2001). The temperature structure of the 2D thread is specified

empirically so as to describe the central cool part of the prominence fine structures and the prominence-corona transition region (PCTR). The PCTR exhibits two different variations of the temperature with a steep temperature gradient in the direction across the magnetic field lines within a narrow PCTR layer and a gradual increase of the temperature from the cool central part of the thread towards its boundaries in the direction along the field lines in which the PCTR is much more extended. This approach is taken into account for the large difference in the heat conduction along and across the magnetic field. The temperature structure of individual models is characterized by four input parameters: the minimum temperature in the centre of the thread T_0 , the maximum transition region temperature T_{tr} at the thread boundaries (index tr stands for transition region), and by two exponents γ_1 and γ_2 describing the gradients of the temperature within the PCTR with γ_2 prescribing the very steep temperature gradient across the field lines and γ_1 representing the gradual rise of the temperature along the field lines from the thread centre towards its boundaries. The other input parameters describing the plasma structure of the 2D thread are $B_x(0)$ representing the magnetic field strength in the middle of the thread, M_0 , which gives the maximum column density, and p_{tr} , which is the value of the gas pressure at the thread boundaries. The geometrical dimensions of the thread are determined in the following way: the length of the thread in the x -direction (along the magnetic field lines) results from the MHS equilibrium and is unique to each set of model input parameters, while the width of the thread in the y -direction (across the field lines) is chosen

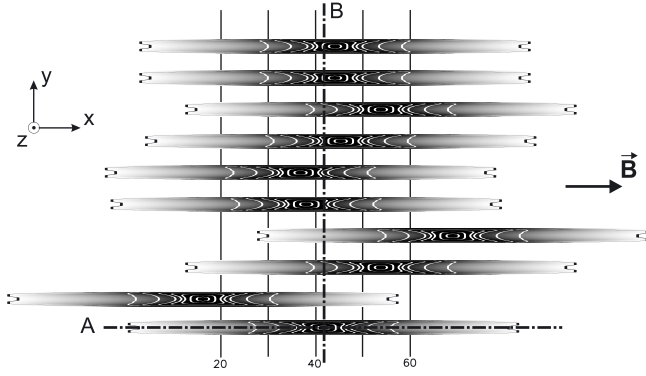


Fig. 3. Vertical projection of a particular multi-thread configuration with randomly shifted threads drawn to proper geometrical scale. The orientation of the magnetic field is indicated by an arrow.

arbitrarily. We chose the value of the thread width to be 1000 km in all our previous modelling and therefore use this value also in this work to maintain consistency. The value of 1000 km was chosen to approximately represent the resolution of the SUMER UV-spectrograph (*Solar Ultraviolet Measurements of Emitted Radiation* – Wilhelm et al. 1995) onboard SOHO (*Solar and Heliospheric Observatory*). However, the observations of quiescent filaments in the hydrogen H- α line (see e.g. Lin et al. 2005) indicate that the widths of the finest structures can be of the order of 100 km. The expressions describing the MHS equilibrium and the temperature structure variation are given in Heinzl & Anzer (2001).

We solve the 2D non-LTE radiative transfer problem in these fine-structure threads to determine the emerging hydrogen spectrum that can be compared with the observed prominence spectra, to derive the parameters of the prominence fine structures (see Gunár et al. 2007, 2008, 2010). By solving the multi-level non-LTE radiative transfer problem within 2D threads, we also determine the proper ionization degree of the hydrogen plasma, thus obtain the variation of the electron density in these 2D prominence fine structure threads. The ionization degree is determined during several iterative steps described in Heinzl & Anzer (2003).

In the present work, we use both single-thread and multi-thread models. Gunár et al. (2007) have shown that the multi-thread models produce synthetic Lyman lines in better agreement with observed ones than can be achieved by using single thread models. This was corroborated by Gunár et al. (2008) who demonstrated the ability of the multi-thread models with randomly assigned LOS velocities of individual threads to reproduce the strong asymmetries of the Lyman lines, a step that could not be achieved by single-thread modelling. We use the multi-thread models consisting of N identical 2D threads without any mutual radiative interaction that were introduced by Gunár et al. (2007). Individual threads of a multi-thread model are arranged perpendicularly to the LOS, along individual field lines (see Fig. 3). Each thread is randomly shifted with respect to the foremost thread with the maximum shift of any thread being equal to half of the length of the thread. These random shifts represent the non-uniformity of the prominence fine structures along any LOS. The LOS therefore intersects individual threads at different positions along the length of each 2D thread, which produces different emerging line profiles, optical thicknesses, etc. In this study, we do not introduce any velocities along the LOS for individual threads into multi-thread modelling (as done by

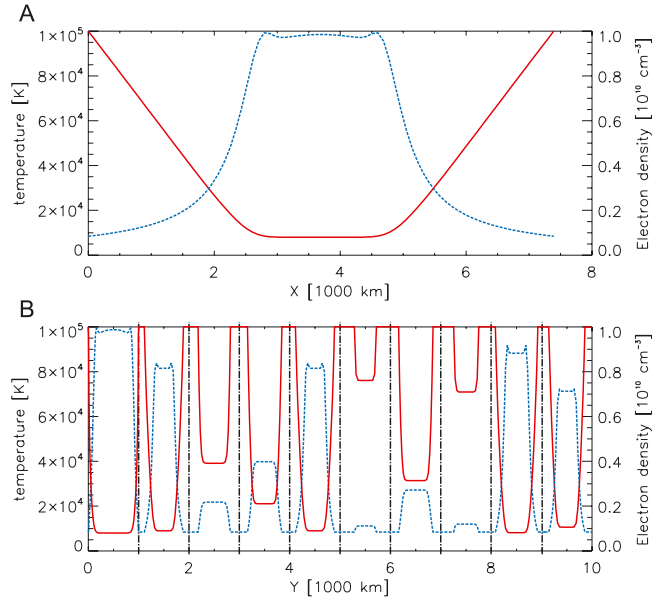


Fig. 4. Temperature (solid red lines) and electron density (dashed blue lines) variation for MODEL2 along cut A (along the magnetic field) and cut B (across the field) indicated in Fig. 3. For multi-thread configuration (cut B), we do not show any gap between threads. The thread boundaries are indicated by dot-dashed lines.

Gunár et al. 2008) because the LOS velocities have no influence on the synthetic DEM curves.

2.1. Parameters of the models used

For this theoretical study of the synthetic DEM curves, we selected two different models that produce synthetic hydrogen Lyman spectra in good agreement with two different observed prominences. MODEL1 corresponds to the prominence observed on May 25 and 26, 2005 and its input parameters were determined by Gunár et al. (2007). MODEL1 was also used for a study of the Lyman line asymmetries by Gunár et al. (2008) and in a statistical analysis of Gunár et al. (2010). MODEL2 was constructed to describe the prominence observed on April 26, 2007 and discussed in Berlicki et al. (2011). All the input parameters of these models are listed in Table 1. The values of the minimum central temperature T_0 , the magnetic field strength in the middle of the thread $B_x(0)$, the maximum column density M_0 , and the boundary gas pressure p_{tr} are in the range of values to be expected in the conditions of the quiescent prominences (see review of Labrosse et al. 2010). The central gas pressure p_{cen} was determined by the MHS equilibrium. The boundary temperature T_{tr} was chosen for both models to be equal to 10^5 K, which is well above the temperature where hydrogen is fully ionized.

The variations of the temperature and electron density are displayed in Figs. 1 and 2. Note that these plots are not drawn to the proper geometrical scale. The 2D threads are actually much more extended in the x -direction (along the field lines).

3. Synthetic DEM curves

The 2D prominence fine-structure thread models provide us with the temperature and electron density variations (see Figs. 1, 2, and 4), so allow us to directly derive the synthetic DEM of the model prominence fine structure. To do this, we divide the temperature range into a number of temperature bins T_i (where

Table 1. List of input parameters of MODEL1 and MODEL2.

MODEL1	$T_0 = 7000 \text{ K}; T_{\text{tr}} = 10^5 \text{ K};$	$\gamma_1 = 10$ $\gamma_2 = 60$
	$B_x(0) = 6 \text{ Gauss}; M_0 = 1.1 \times 10^{-4} \text{ g cm}^{-2};$ $p_{\text{tr}} = 0.015 \text{ dyn cm}^{-2}; p_{\text{cen}} = 0.4 \text{ dyn cm}^{-2}$	
MODEL2	$T_0 = 8000 \text{ K}; T_{\text{tr}} = 10^5 \text{ K};$	$\gamma_1 = 5$ $\gamma_2 = 30$
	$B_x(0) = 5 \text{ Gauss}; M_0 = 1 \times 10^{-5} \text{ g cm}^{-2};$ $p_{\text{tr}} = 0.03 \text{ dyn cm}^{-2}; p_{\text{cen}} = 0.035 \text{ dyn cm}^{-2}$	

T_i goes from T_{min} to T_{max}) of bin-width ΔT_i for a given LOS. Because the temperature profile of a single-thread and a multi-thread model is not a monotonic function along any given LOS (see Fig. 4), we encounter multiple regions at the same temperature along a given LOS that all contribute to the DEM at that temperature. For a sufficiently small temperature bin-width ΔT_i , we then obtain the following formula for DEM(T_i)

$$\text{DEM}(T_i) = \sum_m n_{e(i,m)}^2 \frac{\Delta h_{i,m}}{\Delta T_i}, \quad (3)$$

where $\Delta h_{i,m}$ is the geometrical length of a LOS segment corresponding to the temperature bin $\langle T_i, T_i + \Delta T_i \rangle$ of the region m , and $n_{e(i,m)}$ represents the mean value of the electron density at the LOS segment $\Delta h_{i,m}$. We sum over all regions with the same temperature T_i along a given LOS (see also Frazin et al. 2005). This method of direct numerical DEM computation does not depend on the choice of the temperature bin-width ΔT_i as long as this is sufficiently small. It also does not suffer from the effects of averaging the electron density over extended heterogeneous areas (see Judge 2000) because we use averaged values only over small LOS segments $\Delta h_{i,m}$.

We compute the synthetic DEM of the prominence fine-structure models in the range between the minimum central temperature 7000 K or 8000 K, respectively, and the boundary temperature of 10^5 K. To obtain the DEM curve representing the whole single-thread or multi-thread model, which can be compared with the DEM curves derived from the observations, we compute the average DEM curve over the length or the width of the 2D thread. To be able to accurately describe the thread plasma temperature distribution, it is important to derive the DEM for a large number of lines of sight spanning the given thread dimension. The geometrical distance between individual lines of sight should be comparable to the smallest lengths $\Delta h_{i,m}$ of a LOS segment corresponding to the temperature bin $\langle T_i, T_i + \Delta T_i \rangle$. Because the gradient of temperature across the magnetic field lines is very steep, it is necessary to use a high number of densely placed lines of sight to obtain the synthetic DEM curve for observations along field lines. In this case, we used 50 000 specific LOS equidistantly distributed over the 1000 km width of the thread. The resulting average DEM curve is a smooth and monotonic function on the given temperature interval and comparable to the DEM curves derived from the observations, which also represent the mean DEM of the observed part of the specific prominence.

3.1. Results

For this theoretical study, we selected two models, MODEL1 and MODEL2, which produce synthetic spectra that are in good agreement with the observed spectra of two specific prominences. We study the DEM of single-thread models for two different orientations of the 2D thread configuration with respect to the observer – across and along the magnetic field – and ten-component

multi-thread realizations of the selected models for observations across the magnetic field. We chose ten-component multi-thread models because the MODEL1 was also used with a ten-thread configuration in our previous investigations (Gunár et al. 2007, 2008; and Gunár et al. 2010). There it was taken because the total column mass of the multi-thread model with ten threads obtained along the LOS perpendicular to the magnetic field is in good agreement with the prominence values.

To place the synthetic DEM curves in relation to the observations, we use two recently published sets of DEM data derived from observations. The DEM curve of Parenti & Vial (2007) represents the quiescent prominence observed on Oct. 8, 1999. Another DEM data set was derived for the quiescent prominence observed on Nov. 1, 2000 by Cirigliano et al. (2004). In this study, we do not consider other previously determined DEM curves (see e.g. Wiik et al. 1993). We also do not attempt to find a particular prominence fine-structure model producing synthetic DEM curves in detailed agreement with the DEM curves derived from the observations. Our aim instead is to introduce the method we use to obtain the synthetic DEM curves and discuss the basic dependence of the synthetic DEM curves on the input parameters of the model.

In Fig. 5, we display the synthetic DEM curves for MODEL1 (solid lines) and MODEL2 (dashed lines), and the DEM values derived from observations, i.e. Parenti & Vial (2007) as red dash-dotted lines and Cirigliano et al. (2004) as blue crosses. In the left panel, we give the synthetic DEM curves for single-thread models obtained with the LOS parallel to the magnetic field, for both models we average over the thread width of 1000 km. In the middle panel, we show synthetic DEM curves for single-thread models obtained with the LOS perpendicular to the magnetic field. We average the synthetic DEM over the length of the thread, which is determined by the MHS equilibrium requirement and is different for the two models considered. In this case, the length of MODEL1 is approximately 28 000 km and that of MODEL2 is about 8000 km. In the right panel, we display the synthetic DEM curves for multi-thread models with 10 randomly shifted threads. Here we average along the length of the foremost thread, i.e. 28 000 km for MODEL1 and 8000 km for MODEL2. Similarly, in Fig. 6 we display synthetic DEM curves for three modifications of MODEL2 where we have varied the value of the boundary pressure p_{tr} . We again display the DEM curves for single-thread models obtained with the LOS parallel to the magnetic field in the left panel and with the LOS perpendicular to the field in the middle panel. In the right panel, we show the synthetic DEM curves for multi-thread models with the LOS perpendicular to the magnetic field.

There are two features of the DEM curves, which can reveal some details about the structure of the prominence plasma. The first is the slope of the DEM curves which indicates the respective amount of plasma at given temperatures and so gives information about the temperature structure of the quiescent prominences, especially the temperature gradients within the PCTR. The second feature is the absolute value of the DEM, which indicates the amount of the prominence mass along the LOS. Using these two basic characteristics, we can relate the observed to the synthetic DEM curves. Note that the DEM curves are usually drawn on a log-log scale, which means that small differences deduced from the plots can actually correspond to much larger differences in the real values.

The observed DEM curves can vary significantly from one prominence to another. At temperatures between 20 000 K and 30 000 K, the two prominences observed by Parenti & Vial (2007) and Cirigliano et al. (2004) have similar values

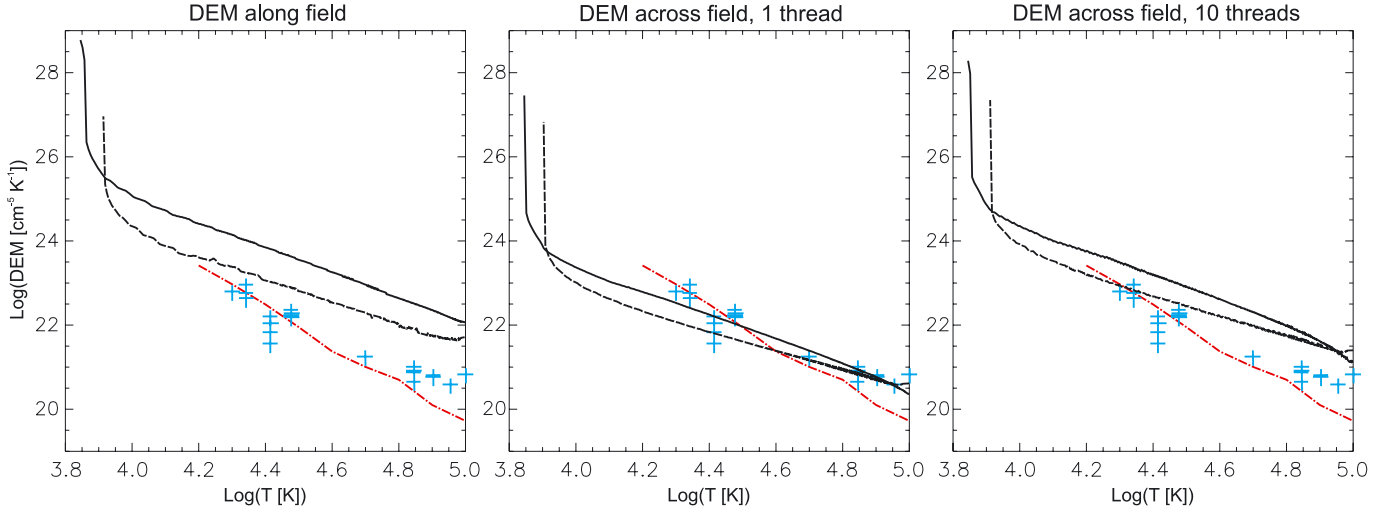


Fig. 5. Synthetic DEM curves for MODEL1 (solid lines) and MODEL2 (dashed lines), and the DEM values derived from observations from Parenti & Vial (2007) (red dash-dotted line) and Cirigliano et al. (2004) (blue crosses). The *left panel* displays the synthetic DEM curves for single-thread models obtained with the LOS parallel to the magnetic field. The *middle panel* shows synthetic DEM curves for single-thread models obtained with the LOS perpendicular to the magnetic field. The *right panel* displays the synthetic DEM curves for multi-thread models each with ten randomly shifted threads.

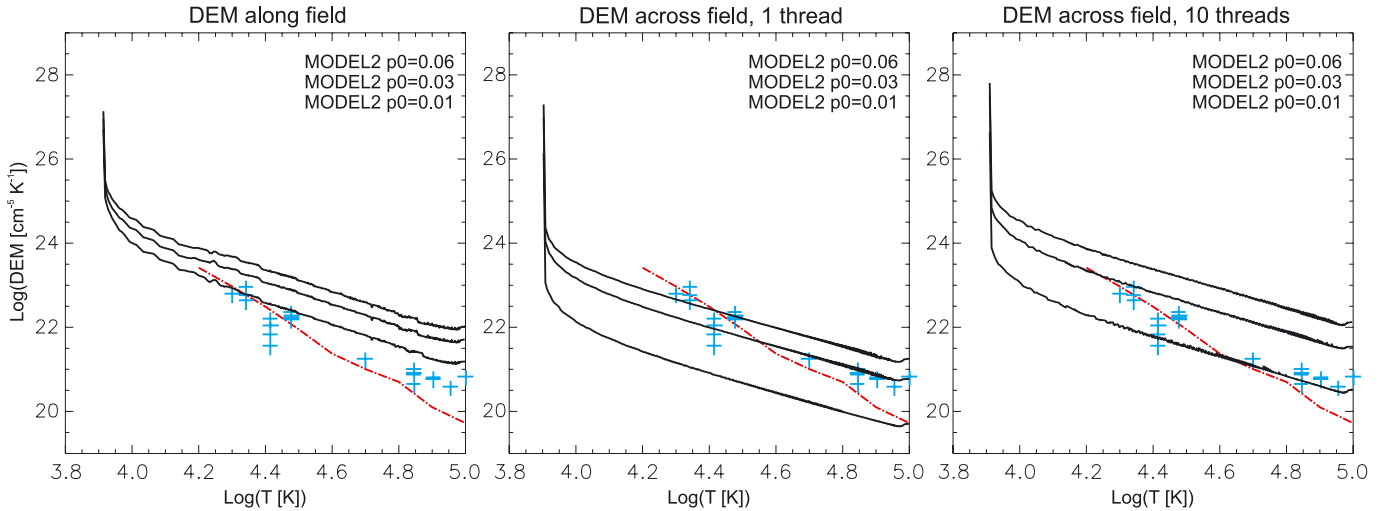


Fig. 6. Same as in Fig. 5 but here we display synthetic DEM curves for three variations of the MODEL2.

of the DEM (see Fig. 5). But at temperatures around 10^5 K, Cirigliano et al. derive ten times larger values for the DEM than Parenti & Vial. This clearly shows that the PCTR can vary quite dramatically from prominence to prominence, and that the temperature structure of these PCTRs has to be different.

The synthetic DEM curves of the MODEL1 and all variations of the MODEL2 (see Figs. 5 and 6) are generally less steep than the DEM curves obtained from the observations, and particularly the one of Parenti & Vial (2007). This implies that either the variation of the temperature gradients in the PCTRs of these observed prominences is much larger than we presently use in the modelling, or the amount of the prominence plasma at the regions with higher temperatures is much lower (the electron density decreases faster with increasing temperature) than what we presently use. The values of the synthetic DEM curves are also globally much larger than the observed ones when calculated along the field lines (left panels of Figs. 5 and 6) and also for most ten-component multi-thread models (right panels of Figs. 5 and 6). Only relatively low gas-pressure models with small column densities, such as MODEL2 (see Fig. 6) give DEM

values corresponding to the observed ones but the gradient of the synthetic DEM curve still disagrees with the DEM curves derived from the observations.

The differences between the synthetic DEM curves of individual models imply that the shapes of the DEM curves depend on the choice of the model input parameters. Figure 5 shows that the DEM curves of the MODEL1 are in all cases much higher than those of the MODEL2. This reflects the fact that the MODEL1 is more massive than the MODEL2 (M_0 of the MODEL1 is an order of magnitude higher). The slope of the DEM curves of MODEL1 is also steeper than that of MODEL2 because of the higher values of the parameters γ_1 and γ_2 of MODEL2, describing the temperature variations in the PCTR along and across the magnetic field, respectively. However, even with rather steep gradients, as in the case of MODEL1, the slope of the synthetic DEM curves is insufficiently steep to match the observed DEM curves of these two particular prominences. The effect of the choice of boundary gas pressure p_{tr} on the shape of the DEM curves is clearly illustrated in Fig. 6. The parameter p_{tr} in addition to both $B_x(0)$ and M_0 determine, assuming MHS equilibrium, the overall pres-

sure structure of the thread and define the amount of prominence plasma in the regions with high temperatures. As is clear from Fig. 6, the higher the boundary gas pressure, the higher the DEM values of the model. The multi-thread models (see right panels of Figs. 5 and 6) exhibit much higher overall DEM values than the single-thread models (central panels), but these do not scale with the number of threads and in the case of the ten-component multi-thread models the DEM values are generally less than a factor of five higher. This is due to the random shifts between individual threads, which can be as large as half of the thread length in the direction along the magnetic field. This implies that for a 20-component multi-thread model the synthetic DEM values would be a factor of two larger than in the case of the ten-component model.

The synthetic DEM curves for single-thread models obtained with the LOS parallel to the magnetic field (left panels of Figs. 5 and 6) and for ten-component multi-thread models with the LOS perpendicular to the field (right panels) are very similar. This demonstrates that the DEM cannot be used to determine the proper spatial distribution of the plasma along any LOS. As we demonstrate here, two completely different temperature and electron density distributions along a given LOS, one with two wide PCTR regions with shallow temperature gradients and the other with 20 very narrow PCTRs with very steep temperature gradients (see Fig. 4) can lead to very similar DEM curves.

4. Discussion and conclusions

Although we have not attempted in this paper to derive one particular prominence fine-structure model that can give synthetic DEM curves in reasonable agreement with those obtained from observations, our analysis has demonstrated that the models that produce the synthetic Lyman line spectra consistent with the observed ones lead to synthetic DEM curves that are similar to those derived from some observations of quiescent prominences.

The derivation of the DEM curves from the existing observations is limited by the fact that only the optically thin UV and EUV lines can be used for the inversion technique (see Avrett 2007). Since all these lines originate in regions of temperatures above 20 000 K, these DEM curves are reliable only above these temperatures. On the other hand, our multi-thread models have been designed to reproduce the observed hydrogen Lyman spectra, which originate mainly at temperatures below 20 000 K. Thus, we expect that the temperature and density structures of our models at temperatures below 20 000 K agree with those of the observed prominences and therefore that the resulting synthetic DEM curves would correspond to the observed prominence structure at these lower temperatures. The synthetic DEM curves obtained by this forward modelling using some assumed temperature and electron density distributions of the prominence fine structures can therefore provide DEM curves extending from 20 000 K all the way to the minimum temperature at the centre of the fine structures and one can in this way extend the DEM curves previously derived from the observations by applying inversion techniques.

On the other hand, the DEM curves derived from the observations can be used as a constraint on the temperature structure of our prominence fine-structure models at those temperatures that lie above the formation temperature of the Lyman lines, where our models use a rather arbitrary PCTR structure. However, the observed DEM cannot provide us with detailed information on the spatial distribution

of the temperature (and electron density) inside the PCTR. By comparing the synthetic DEM curves obtained in this way with those derived from observations, we have been able to modify the empirical temperature structure of our prominence fine-structure models above the formation temperature of the Lyman lines to be consistent with the observations. To this end, one could use the synthetic DEM curves together with the CHIANTI database (Dere et al. 2009) for the synthesis of the optically thin lines originating in the PCTR. A direct comparison of the intensities of the synthetic spectral lines with those in the observed spectra could then be used to analyse of the structure of the prominence plasma inside the PCTR. We plan to apply this forward modelling technique in a future investigation, where we shall concentrate on particular SOHO/SUMER data sets where both the Lyman lines were observed in detail and also the intensities of the optically thin high temperature lines in the PCTR have been determined. We shall also consider the energy balance in multi-thread structures, by extending the ideas of Anzer & Heinzel (2008).

Acknowledgements. S.G. acknowledges the support from grant 250/09/P554 of the Grant Agency of the Czech Republic. P.H. acknowledges the support from grant 205/09/1705 and 209/10/1706 of the Grant Agency of the Czech Republic. S.G. and P.H. acknowledge the support from the MPA Garching; U.A. thanks for support from the Ondřejov Observatory. The authors acknowledge support from the International Space Science Institute, Bern, Switzerland to the International Team 174. This work was also supported by ESA-PECS project No. 98030 and the institutional project AVOZ10030501.

References

- Anzer, U., & Heinzel, P. 1999, A&A, 349, 974
 Anzer, U., & Heinzel, P. 2000, A&A, 358, L75
 Anzer, U., & Heinzel, P. 2008, A&A, 480, 537
 Avrett, E. H. 2007, in *The Physics of Chromospheric Plasmas*, ed. P. Heinzel, I. Dorotovič, & R. J. Rutten, ASP Conf. Ser., 368, 81
 Berlicki, A., Gunár, S., Heinzel, P., Schmieder, B., & Schwartz, P. 2011, A&A, accepted
 Chiuderi Drago, F., Engvold, O., & Jensen, E. 1992, Sol. Phys., 139, 47
 Cirigliano, D., Vial, J., & Rovira, M. 2004, Sol. Phys., 223, 95
 Dere, K. P., Landi, E., Young, P. R., et al. 2009, A&A, 498, 915
 Engvold, O. 1988, in *Solar and Stellar Coronal Structure and Dynamics*, ed. R. C. Altrock, 151
 Frazin, R. A., Kamalabadi, F., & Weber, M. A. 2005, ApJ, 628, 1070
 Gunár, S., Heinzel, P., Schmieder, B., Schwartz, P., & Anzer, U. 2007, A&A, 472, 929
 Gunár, S., Heinzel, P., Anzer, U., & Schmieder, B. 2008, A&A, 490, 307
 Gunár, S., Schwartz, P., Schmieder, B., Heinzel, P., & Anzer, U. 2010, A&A, 514, A43
 Heinzel, P., & Anzer, U. 2001, A&A, 375, 1082
 Heinzel, P., & Anzer, U. 2003, in *Stellar Atmosphere Modeling*, ed. I. Hubeny, D. Mihalas, & K. Werner, ASP Conf. Ser., 288, 441
 Judge, P. G. 2000, ApJ, 531, 585
 Kippenhahn, R., & Schlüter, A. 1957, *Zeitschrift für Astrophysik*, 43, 36
 Labrosse, N., Heinzel, P., Vial, J., et al. 2010, Space Sci. Rev., 151, 243
 Lin, Y., Engvold, O., Rouppe van der Voort, L., Wiik, J. E., & Berger, T. E. 2005, Sol. Phys., 226, 239
 Mariska, J. T. 1992, *The Solar Transition Region*, ed. Mariska, J. T., Cambridge Astrophysics Series (New York: Cambridge University Press)
 Orrall, F. Q., & Schmahl, E. J. 1976, Sol. Phys., 50, 365
 Parenti, S., & Vial, J.-C. 2007, A&A, 469, 1109
 Patsourakos, S., & Vial, J.-C. 2002, Sol. Phys., 208, 253
 Phillips, K. J. H., Feldman, U., & Landi, E. 2008, *Ultraviolet and X-ray Spectroscopy of the Solar Atmosphere*, ed. K. J. H. Phillips, U. Feldman, & E. Landi (Cambridge University Press)
 Tandberg-Hanssen, E. 1995, *The nature of solar prominences* (Dordrecht, Boston: Kluwer)
 Wiik, J. E., Dere, K., & Schmieder, B. 1993, A&A, 273, 267
 Wilhelm, K., Curdt, W., Marsch, E., et al. 1995, Sol. Phys., 162, 189